SCIENCE CHINA
Information Sciences

• RESEARCH PAPER •

May 2023, Vol. 66 152306:1–152306:12
https://doi.org/10.1007/s11432-022-3540-5

Persymmetric adaptive detection of range-spread targets in subspace interference plus Gaussian clutter

Tao JIAN*, Jia HE, Yu LIU, You HE, Congan XU & Zikeng XIE

Research Institute of Information Fusion, Naval Aviation University, Yantai 264001*, China*

Received 29 January 2022/Revised 22 April 2022/Accepted 28 June 2022/Published online 20 April 2023

Abstract In this paper, we consider the adaptive detection problem of range-spread targets embedded in subspace interference plus structured Gaussian clutter. The target signal and interference are assumed to lie in two linearly independent subspaces with unknown coordinates. The clutter component is modeled as a complex Gaussian vector with an unknown persymmetric covariance matrix. We leverage the persymmetric structure to design a two-step detector according to the Rao test criterion. The theoretical results show that the proposed detector possesses the constant false alarm rate property with respect to the clutter covariance matrix. Furthermore, the numerical results show that the proposed detector exhibits better detection performance than the existing unstructured subspace detectors, particularly under a limited training data size. In addition, the proposed detector outperforms the existing persymmetric subspace detectors.

Keywords adaptive detection, persymmetry, structured interference, constant false alarm rate, Rao test

Citation Jian T, He J, Liu Y, et al. Persymmetric adaptive detection of range-spread targets in subspace interference plus Gaussian clutter. Sci China Inf Sci, 2023, 66(5): 152306, https://doi.org/10.1007/s11432-022-3540-5

1 Introduction

With the increasing radar bandwidth, the adaptive detection of the wideband radar target has become a crucial problem in the radar community [1,2]. The spreading of the wideband radar target energy into the adjacent range cells [3–5] results in the so-called range-spread target. Moreover, multichannel adaptive target detection in Gaussian clutter with an unknown covariance matrix has been an active topic [6–8], and a set of target-free training data is usually assumed to be available to estimate unknown clutter covariance matrices. However, natural or man-made interference sources are frequently encountered in several applications, such as electronic countermeasures or civil broadcasting systems. The interference must be considered in the detector design, and the subspace model [9, 10] is usually applied to describe the uncertainties associated with interference pointing and Doppler frequency in many scenarios.

Several detectors have been designed to detect range-spread targets embedded in subspace interference plus colored Gaussian clutter using sufficient amounts of training data, according to the generalized likelihood ratio test (GLRT) [11] or the Rao test [12]. Moreover, in [13], a relative parameter is set to comprise both signal coordinates and interference coordinates to derive a modified Rao (MRao) test.

None of the above-mentioned detectors consider the persymmetry of the clutter covariance matrix, which may exist in radar systems utilizing a symmetrically spaced linear array or symmetrically spaced pulse trains [14, 15]. In some scenarios, special structures may exist in the clutter covariance matrix. A persymmetric structure is characterized by a Hermitian symmetry about its principal diagonal and persymmetry about its sub diagonal. In particular, the persymmetric structure of the clutter covariance matrix has been considered for the detection problem [11], and one-step and two-step detectors are proposed in [14], according to the GLRT criterion. In [14], the persymmetric one-step GLRT (P1S-GLRT) generally exhibited better detection performance than the two-step GLRT.

In the case in which the clutter covariance matrix and the coordinates of the target signal and interference are unknown, it is difficult to obtain a uniformly most powerful test for the detection problem [14].

* Corresponding author (email: work_jt@163.com)

The aim of this paper is to leverage persymmetry to propose a two-step detector according to the Rao test criterion. Moreover, the proposed persymmetric two-step Rao (P2S-Rao) is theoretically proved to achieve a constant false alarm rate (CFAR) with respect to the unknown clutter covariance matrix. The numerical results show that the P2S-Rao can effectively reject the interference. Furthermore, the P2S-Rao has a better detection performance than the existing unstructured subspace detectors [11–13], particularly under a limited training data size. Moreover, the proposed P2S-Rao outperforms the existing persymmetric subspace detectors in [14].

The rest of this paper is organized as follows. Section 2 presents the formulation of the detection problem. Section 3 provides the derivation of the P2S-Rao detector. Section 4 presents the CFAR property analysis. Section 5 presents the numerical analyses and performance comparison. Finally, Section 6 presents the conclusion of the study.

2 Problem formulation

The problem of detecting the presence of a target across K range cells can be formulated in terms of two hypotheses: H_0 and H_1. The hypothesis H_0 contains interference and clutter only, and the hypothesis H_1 contains useful target signals. Under hypothesis H_1, the data from the tested cells can be expressed as

$$\dot{\boldsymbol{z}}_t = \dot{\boldsymbol{s}}_t + \dot{\boldsymbol{j}}_t + \dot{\boldsymbol{c}}_t, \tag{1}$$

where the target signal vector $\dot{\boldsymbol{s}}_t \in \mathbb{C}^{N\times 1}$ and the interference vector $\dot{\boldsymbol{j}}_t \in \mathbb{C}^{N\times 1}$ are assumed to be deterministic, and $\mathbb{C}^{m\times n}$ denotes the $m \times n$ complex-valued matrix space. It is supposed that $\dot{\boldsymbol{s}}_t$ and $\dot{\boldsymbol{j}}_t$ belong to known full-column-rank unitary matrices $\dot{\boldsymbol{H}} \in \mathbb{C}^{N\times p}$ and $\dot{\boldsymbol{J}} \in \mathbb{C}^{N\times q}$, and can be denoted by $\dot{\boldsymbol{s}}_t = \dot{\boldsymbol{H}}\boldsymbol{p}_t$ and $\dot{\boldsymbol{j}}_t = \dot{\boldsymbol{J}}\boldsymbol{q}_t$, respectively, where two vectors $\boldsymbol{p}_t \in \mathbb{C}^{p\times 1}$ and $\boldsymbol{q}_t \in \mathbb{C}^{q\times 1}$ are unknown coordinate vectors for the target signal and the interference signal, respectively. The subspaces $\dot{\boldsymbol{H}}$ and $\dot{\boldsymbol{J}}$ are supposed to be linearly independent [11], and $\dot{\boldsymbol{B}} = [\dot{\boldsymbol{H}}\ \dot{\boldsymbol{J}}]$ is a full-column-rank augmented matrix such that $p + q < N$. The clutter vectors $\dot{\boldsymbol{c}}_t, t = 1, 2, \ldots, K$ are independent and identically distributed (IID), zero-mean, complex circular Gaussian vectors, with an unknown covariance matrix $\dot{\boldsymbol{M}}$; they are defined as $\dot{\boldsymbol{c}}_t \sim \mathcal{CN}(0, \dot{\boldsymbol{M}})$. Under hypothesis H_0, $\dot{\boldsymbol{z}}_t = \dot{\boldsymbol{j}}_t + \dot{\boldsymbol{c}}_t$. To estimate $\dot{\boldsymbol{M}}$, it is often assumed that a set of training data containing clutter only is available. The training data are defined as an $N \times R$ matrix $\dot{\boldsymbol{Y}} = [\dot{\boldsymbol{y}}_1, \ldots, \dot{\boldsymbol{y}}_R]$, with $\dot{\boldsymbol{y}}_t \sim \mathcal{CN}(0, \dot{\boldsymbol{M}}), t = 1, 2, \ldots, R$ being also IID.

According to the above assumption, the detection problem can be formulated as the following binary hypothesis test:

$$\begin{cases} \mathrm{H}_0 : \begin{cases} \dot{\boldsymbol{z}}_t \sim \mathcal{CN}(\dot{\boldsymbol{J}}\boldsymbol{q}_t, \dot{\boldsymbol{M}}), & t = 1, 2, \ldots, K, \\ \dot{\boldsymbol{y}}_t \sim \mathcal{CN}(\boldsymbol{0}, \dot{\boldsymbol{M}}), & t = 1, 2, \ldots, R, \end{cases} \\ \mathrm{H}_1 : \begin{cases} \dot{\boldsymbol{z}}_t \sim \mathcal{CN}(\dot{\boldsymbol{H}}\boldsymbol{p}_t + \dot{\boldsymbol{J}}\boldsymbol{q}_t, \dot{\boldsymbol{M}}), & t = 1, 2, \ldots, K, \\ \dot{\boldsymbol{y}}_t \sim \mathcal{CN}(\boldsymbol{0}, \dot{\boldsymbol{M}}), & t = 1, 2, \ldots, R. \end{cases} \end{cases} \tag{2}$$

When a symmetrically spaced linear array with its center at the origin or symmetrically spaced pulse trains is used [14–16], $\dot{\boldsymbol{H}}$, $\dot{\boldsymbol{J}}$ and $\dot{\boldsymbol{M}}$ have persymmetric structures. In this case, we have

$$\begin{cases} \dot{\boldsymbol{H}} = \boldsymbol{D}_N \dot{\boldsymbol{H}}^* \in \mathbb{C}^{N\times p}, \\ \dot{\boldsymbol{J}} = \boldsymbol{D}_N \dot{\boldsymbol{J}}^* \in \mathbb{C}^{N\times q}, \\ \dot{\boldsymbol{M}} = \boldsymbol{D}_N \dot{\boldsymbol{M}}^* \boldsymbol{D}_N \in \mathbb{C}^{N\times N}, \end{cases} \tag{3}$$

where the superscript $(\cdot)^*$ denotes the conjugate; $\boldsymbol{D}_N$ is an $N \times N$ permutation matrix with unit antidiagonal elements and zeros elsewhere.

3 Detector design

To leverage the persymmetric structure, we convert the complex-valued matrices $\dot{\boldsymbol{H}}$, $\dot{\boldsymbol{J}}$ and $\dot{\boldsymbol{M}}$ to real-valued matrices by applying a unitary matrix $\boldsymbol{T}$ [7], which can be expressed as

$$\boldsymbol{T}=\begin{cases}\frac{1}{\sqrt{2}}\begin{pmatrix}\boldsymbol{I}_{N/2} & \boldsymbol{D}_{N/2}\\ \mathrm{j}\boldsymbol{I}_{N/2} & -\mathrm{j}\boldsymbol{D}_{N/2}\end{pmatrix}, & \text{for even } N,\\ \frac{1}{\sqrt{2}}\begin{pmatrix}\boldsymbol{I}_{(N-1)/2} & 0 & \boldsymbol{D}_{(N-1)/2}\\ 0 & \sqrt{2} & 0\\ \mathrm{j}\boldsymbol{I}_{(N-1)/2} & 0 & -\mathrm{j}\boldsymbol{D}_{(N-1)/2}\end{pmatrix}, & \text{for odd } N.\end{cases} \tag{4}$$

where $\boldsymbol{I}_m$ denotes an $m\times m$ unit matrix, $\mathrm{j}=\sqrt{-1}$, and the binary hypothesis test can be rewritten as

$$\begin{cases}\mathrm{H}_0:\begin{cases}\boldsymbol{z}_t\sim\mathcal{CN}\left(\boldsymbol{J}\boldsymbol{q}_t,\boldsymbol{M}\right), & t=1,2,\ldots,K,\\ \boldsymbol{y}_t\sim\mathcal{CN}\left(\boldsymbol{0},\boldsymbol{M}\right), & t=1,2,\ldots,R,\end{cases}\\ \mathrm{H}_1:\begin{cases}\boldsymbol{z}_t\sim\mathcal{CN}\left(\boldsymbol{H}\boldsymbol{p}_t+\boldsymbol{J}\boldsymbol{q}_t,\boldsymbol{M}\right), & t=1,2,\ldots,K,\\ \boldsymbol{y}_t\sim\mathcal{CN}\left(\boldsymbol{0},\boldsymbol{M}\right), & t=1,2,\ldots,R,\end{cases}\end{cases} \tag{5}$$

with

$$\begin{cases}\boldsymbol{z}_t=\boldsymbol{T}\dot{\boldsymbol{z}}_t\in\mathbb{C}^{N\times 1},\\ \boldsymbol{y}_t=\boldsymbol{T}\dot{\boldsymbol{y}}_t\in\mathbb{C}^{N\times 1},\\ \boldsymbol{H}=\boldsymbol{T}\dot{\boldsymbol{H}}\in\mathbb{R}^{N\times p},\\ \boldsymbol{J}=\boldsymbol{T}\dot{\boldsymbol{J}}\in\mathbb{R}^{N\times q},\\ \boldsymbol{M}=\boldsymbol{T}\dot{\boldsymbol{M}}\boldsymbol{T}^{\mathrm{H}}\in\mathbb{R}^{N\times N},\end{cases} \tag{6}$$

where the superscript $(\cdot)^{\mathrm{H}}$ denotes the conjugate transpose, and $\mathbb{R}^{m\times n}$ denotes the $m\times n$ real-valued matrix space.

In the sequel, we adopt the two-step criterion to design a Rao test for the detection problem in (5). First, we assume that the clutter covariance matrix $\boldsymbol{M}$ is known and derive a detection statistic. Then, we obtain the maximum likelihood (ML) estimate of the persymmetric matrix $\boldsymbol{M}$ using the training data, which are then used to replace the true matrix $\boldsymbol{M}$ in the previously derived detection statistic.

The joint probability density function of $\boldsymbol{Z}=[\boldsymbol{z}_1,\ldots,\boldsymbol{z}_K]$ and $\boldsymbol{Y}=[\boldsymbol{y}_1,\ldots,\boldsymbol{y}_R]$ under hypotheses H_0 and H_1 can be respectively expressed as [12]

$$f_0(\boldsymbol{Z},\boldsymbol{Y}\,|\boldsymbol{Q},\boldsymbol{M})=\{\pi^{N(K+R)}[\det(\boldsymbol{M})]^{K+R}\}^{-1}\exp\{-\mathrm{tr}(\boldsymbol{M}^{-1}\boldsymbol{S})-\mathrm{tr}[\boldsymbol{M}^{-1}(\boldsymbol{Z}-\boldsymbol{J}\boldsymbol{Q})(\boldsymbol{Z}-\boldsymbol{J}\boldsymbol{Q})^{\mathrm{H}}]\} \tag{7}$$

and

$$f_1(\boldsymbol{Z},\boldsymbol{Y}\,|\boldsymbol{P},\boldsymbol{Q},\boldsymbol{M})=\{\pi^{N(K+R)}[\det(\boldsymbol{M})]^{K+R}\}^{-1}\exp\{-\mathrm{tr}(\boldsymbol{M}^{-1}\boldsymbol{S})-\mathrm{tr}[\boldsymbol{M}^{-1}(\boldsymbol{Z}-\boldsymbol{B}\boldsymbol{D})(\boldsymbol{Z}-\boldsymbol{B}\boldsymbol{D})^{\mathrm{H}}]\}, \tag{8}$$

where $\boldsymbol{P}=[\boldsymbol{p}_1,\ldots,\boldsymbol{p}_K]$; $\boldsymbol{Q}=[\boldsymbol{q}_1,\ldots,\boldsymbol{q}_K]$; $\boldsymbol{S}=\boldsymbol{Y}\boldsymbol{Y}^{\mathrm{H}}$; $\boldsymbol{B}=[\boldsymbol{H}\ \boldsymbol{J}]$; $\boldsymbol{D}=[\boldsymbol{P}^{\mathrm{T}}\ \boldsymbol{Q}^{\mathrm{T}}]^{\mathrm{T}}$; the superscript $(\cdot)^{\mathrm{T}}$ denotes the transpose; and $\det(\cdot)$ and $\mathrm{tr}(\cdot)$ denote the determinant and trace of a square matrix, respectively.

First, for a known $\boldsymbol{M}$, the Rao test for complex-valued signals is given by

$$\lambda_1=\left.\frac{\partial\ln f_1(\boldsymbol{Z},\boldsymbol{Y}\,|\boldsymbol{P},\boldsymbol{Q},\boldsymbol{M})}{\partial\boldsymbol{\Theta}_{\mathrm{r}}}\right|^{\mathrm{T}}_{\boldsymbol{\Theta}=\hat{\boldsymbol{\Theta}}_0}[\boldsymbol{I}^{-1}(\hat{\boldsymbol{\Theta}}_0)]_{\boldsymbol{\Theta}_{\mathrm{r}},\boldsymbol{\Theta}_{\mathrm{r}}}\left.\frac{\partial\ln f_1(\boldsymbol{Z},\boldsymbol{Y}\,|\boldsymbol{P},\boldsymbol{Q},\boldsymbol{M})}{\partial\boldsymbol{\Theta}^*_{\mathrm{r}}}\right|_{\boldsymbol{\Theta}=\hat{\boldsymbol{\Theta}}_0}\underset{\mathrm{H}_0}{\overset{\mathrm{H}_1}{\gtrless}}T_1, \tag{9}$$

where λ_1 and T_1 represent the detection statistic and threshold, respectively; $\boldsymbol{\Theta}=[\boldsymbol{\Theta}_{\mathrm{r}}^{\mathrm{T}}\ \boldsymbol{\Theta}_{\mathrm{s}}^{\mathrm{T}}]^{\mathrm{T}}$, $\boldsymbol{\Theta}_{\mathrm{r}}=\mathrm{vec}(\boldsymbol{P})$, $\boldsymbol{\Theta}_{\mathrm{s}}=\mathrm{vec}(\boldsymbol{Q})$ and $\hat{\boldsymbol{\Theta}}_0$ is the ML estimation of $\boldsymbol{\Theta}$ under hypothesis H_0; $\mathrm{vec}(\cdot)$ denotes the vectorization of a matrix; $[\boldsymbol{I}^{-1}(\boldsymbol{\Theta})]_{\boldsymbol{\Theta}_{\mathrm{r}},\boldsymbol{\Theta}_{\mathrm{r}}}$ denotes the sub-matrix of $\boldsymbol{I}^{-1}(\boldsymbol{\Theta})$ corresponding to the vector $\boldsymbol{\Theta}_{\mathrm{r}}$, with $\boldsymbol{I}(\boldsymbol{\Theta})$ denoting the Fisher information matrix (FIM) with respect to $\boldsymbol{\Theta}$ [17]; that is,

$$\boldsymbol{I}(\boldsymbol{\Theta})=\mathrm{E}\left\{\frac{\partial\ln f_1(\boldsymbol{Z},\boldsymbol{Y}\,|\boldsymbol{P},\boldsymbol{Q},\boldsymbol{M})}{\partial\boldsymbol{\Theta}^*}\frac{\partial\ln f_1(\boldsymbol{Z},\boldsymbol{Y}\,|\boldsymbol{P},\boldsymbol{Q},\boldsymbol{M})}{\partial\boldsymbol{\Theta}^{\mathrm{T}}}\right\}. \tag{10}$$

For convenience, the FIM is often partitioned as follows:

$$\boldsymbol{I}(\boldsymbol{\Theta}) = \begin{bmatrix} \boldsymbol{I}_{\boldsymbol{\Theta}_\mathrm{r},\boldsymbol{\Theta}_\mathrm{r}}(\boldsymbol{\Theta}) & \boldsymbol{I}_{\boldsymbol{\Theta}_\mathrm{r},\boldsymbol{\Theta}_\mathrm{s}}(\boldsymbol{\Theta}) \\ \boldsymbol{I}_{\boldsymbol{\Theta}_\mathrm{s},\boldsymbol{\Theta}_\mathrm{r}}(\boldsymbol{\Theta}) & \boldsymbol{I}_{\boldsymbol{\Theta}_\mathrm{s},\boldsymbol{\Theta}_\mathrm{s}}(\boldsymbol{\Theta}) \end{bmatrix}, \tag{11}$$

and $[\boldsymbol{I}^{-1}(\boldsymbol{\Theta})]_{\boldsymbol{\Theta}_\mathrm{r},\boldsymbol{\Theta}_\mathrm{r}}$ can be expressed as

$$[\boldsymbol{I}^{-1}(\boldsymbol{\Theta})]_{\boldsymbol{\Theta}_\mathrm{r},\boldsymbol{\Theta}_\mathrm{r}} = [\boldsymbol{I}_{\boldsymbol{\Theta}_\mathrm{r},\boldsymbol{\Theta}_\mathrm{r}}(\boldsymbol{\Theta}) - \boldsymbol{I}_{\boldsymbol{\Theta}_\mathrm{r},\boldsymbol{\Theta}_\mathrm{s}}(\boldsymbol{\Theta})\boldsymbol{I}^{-1}_{\boldsymbol{\Theta}_\mathrm{s},\boldsymbol{\Theta}_\mathrm{s}}(\boldsymbol{\Theta})\boldsymbol{I}_{\boldsymbol{\Theta}_\mathrm{s},\boldsymbol{\Theta}_\mathrm{r}}(\boldsymbol{\Theta})]^{-1}. \tag{12}$$

$[\boldsymbol{I}^{-1}(\boldsymbol{\Theta})]_{\boldsymbol{\Theta}_\mathrm{r},\boldsymbol{\Theta}_\mathrm{r}} = [\boldsymbol{I}_{\boldsymbol{\Theta}_\mathrm{r},\boldsymbol{\Theta}_\mathrm{r}}(\boldsymbol{\Theta})]^{-1}$ because $\boldsymbol{I}_{\boldsymbol{\Theta}_\mathrm{r},\boldsymbol{\Theta}_\mathrm{s}}(\boldsymbol{\Theta})$ is a null matrix. Taking the derivatives of the logarithm of (8) with respect to $\boldsymbol{\Theta}_\mathrm{r}$ and $\boldsymbol{\Theta}_\mathrm{r}^*$ results in

$$\frac{\partial \ln f_1(\boldsymbol{Z},\boldsymbol{Y}\,|\boldsymbol{P},\boldsymbol{Q},\boldsymbol{M}\,)}{\partial \boldsymbol{\Theta}_\mathrm{r}} = \mathrm{vec}\left\{[(\boldsymbol{Z}-\boldsymbol{B}\boldsymbol{D})^\mathrm{H}\boldsymbol{M}^{-1}\boldsymbol{H}]^\mathrm{T}\right\}, \tag{13}$$

$$\frac{\partial \ln f_1(\boldsymbol{Z},\boldsymbol{Y}\,|\boldsymbol{P},\boldsymbol{Q},\boldsymbol{M}\,)}{\partial \boldsymbol{\Theta}_\mathrm{r}^*} = \mathrm{vec}[\boldsymbol{H}^\mathrm{T}\boldsymbol{M}^{-1}(\boldsymbol{Z}-\boldsymbol{B}\boldsymbol{D})], \tag{14}$$

respectively. Let $\boldsymbol{X} = \boldsymbol{Z} - \boldsymbol{B}\boldsymbol{D}$; then, plugging (13) and (14) into (10) yields

$$\begin{aligned} \boldsymbol{I}_{\boldsymbol{\Theta}_\mathrm{r},\boldsymbol{\Theta}_\mathrm{r}}(\boldsymbol{\Theta}) &= \mathrm{E}\left[\mathrm{vec}(\boldsymbol{H}^\mathrm{T}\boldsymbol{M}^{-1}\boldsymbol{X})\mathrm{vec}^\mathrm{T}(\boldsymbol{H}^\mathrm{T}\boldsymbol{M}^{-\mathrm{T}}\boldsymbol{X}^*)\right] \\ &= \mathrm{E}\left\{(\boldsymbol{I}_K \otimes \boldsymbol{H}^\mathrm{T}\boldsymbol{M}^{-1})\mathrm{vec}(\boldsymbol{X})[(\boldsymbol{I}_K \otimes \boldsymbol{H}^\mathrm{T}\boldsymbol{M}^{-\mathrm{T}})\mathrm{vec}(\boldsymbol{X}^*)]^\mathrm{T}\right\} \\ &= (\boldsymbol{I}_K \otimes \boldsymbol{H}^\mathrm{T}\boldsymbol{M}^{-1})\mathrm{E}[\mathrm{vec}(\boldsymbol{X})\mathrm{vec}(\boldsymbol{X}^\mathrm{H})](\boldsymbol{I}_K \otimes \boldsymbol{M}^{-1}\boldsymbol{H}) \\ &= (\boldsymbol{I}_K \otimes \boldsymbol{H}^\mathrm{T}\boldsymbol{M}^{-1})(\boldsymbol{I}_K \otimes \boldsymbol{M})(\boldsymbol{I}_K \otimes \boldsymbol{M}^{-1}\boldsymbol{H}) \\ &= \boldsymbol{I}_K \otimes \boldsymbol{H}^\mathrm{T}\boldsymbol{M}^{-1}\boldsymbol{H}, \end{aligned} \tag{15}$$

where $\otimes$ denotes the Kronecker product, and we have used $\mathrm{vec}(\mathbf{ABC}) = (\mathbf{C}^\mathrm{T}\otimes\mathbf{A})\mathrm{vec}(\mathbf{B})$ in the derivation of (15). Substituting (13) and (15) into (9) leads to the Rao test for a given $\boldsymbol{Q}$

$$\begin{aligned} \lambda_1 &= \mathrm{vec}^\mathrm{T}[(\boldsymbol{X}^\mathrm{H}\boldsymbol{M}^{-1}\boldsymbol{H})^\mathrm{T}](\boldsymbol{I}_K \otimes \boldsymbol{H}^\mathrm{T}\boldsymbol{M}^{-1}\boldsymbol{H})^{-1}\mathrm{vec}(\boldsymbol{H}^\mathrm{T}\boldsymbol{M}^{-1}\boldsymbol{X}) \\ &= \mathrm{vec}^\mathrm{T}[(\boldsymbol{X}^\mathrm{H}\boldsymbol{M}^{-1}\boldsymbol{H})^\mathrm{T}][\boldsymbol{I}_K \otimes (\boldsymbol{H}^\mathrm{T}\boldsymbol{M}^{-1}\boldsymbol{H})^{-1}]\mathrm{vec}(\boldsymbol{H}^\mathrm{T}\boldsymbol{M}^{-1}\boldsymbol{X}) \\ &= \mathrm{vec}^\mathrm{T}(\boldsymbol{X}^\mathrm{H}\boldsymbol{M}^{-1}\boldsymbol{H})^\mathrm{T}\mathrm{vec}[(\boldsymbol{H}^\mathrm{T}\boldsymbol{M}^{-1}\boldsymbol{H})^{-1}\boldsymbol{H}^\mathrm{T}\boldsymbol{M}^{-1}\boldsymbol{X}] \\ &= \mathrm{tr}[\boldsymbol{X}^\mathrm{H}\boldsymbol{M}^{-1}\boldsymbol{H}(\boldsymbol{H}^\mathrm{T}\boldsymbol{M}^{-1}\boldsymbol{H})^{-1}\boldsymbol{H}^\mathrm{T}\boldsymbol{M}^{-1}\boldsymbol{X}], \end{aligned} \tag{16}$$

where we have used $(\boldsymbol{A}\otimes\boldsymbol{B})^{-1} = \boldsymbol{A}^{-1}\otimes\boldsymbol{B}^{-1}$ and $\mathrm{tr}(\boldsymbol{A}^\mathrm{T}\boldsymbol{B}) = \mathrm{vec}^\mathrm{T}(\boldsymbol{A})\mathrm{vec}(\boldsymbol{B})$. The ML estimate of $\boldsymbol{Q}$ under hypothesis H_0 can be obtained as [18]

$$\hat{\boldsymbol{Q}}_0 = (\tilde{\boldsymbol{J}}^\mathrm{T}\tilde{\boldsymbol{J}})^{-1}\tilde{\boldsymbol{J}}^\mathrm{T}\tilde{\boldsymbol{Z}}, \tag{17}$$

where $\widetilde{\boldsymbol{Z}} = \boldsymbol{M}^{-1/2}\boldsymbol{Z} \in \mathbb{C}^{N\times K}$ and $\widetilde{\boldsymbol{J}} = \boldsymbol{M}^{-1/2}\boldsymbol{J} \in \mathbb{R}^{N\times q}$.

Note that $\boldsymbol{P}$ is a zero matrix under hypothesis H_0. Substituting (17) into (16) gives

$$\lambda_1 = \mathrm{tr}\left(\tilde{\boldsymbol{Z}}^\mathrm{H}\boldsymbol{P}_{\tilde{\boldsymbol{J}}}^\perp\boldsymbol{P}_{\tilde{\boldsymbol{H}}}\boldsymbol{P}_{\tilde{\boldsymbol{J}}}^\perp\tilde{\boldsymbol{Z}}\right), \tag{18}$$

where $\tilde{\boldsymbol{H}} = \boldsymbol{M}^{-1/2}\boldsymbol{H} \in \mathbb{R}^{N\times p}$, $\boldsymbol{P}_{\tilde{\boldsymbol{H}}} = \tilde{\boldsymbol{H}}(\tilde{\boldsymbol{H}}^\mathrm{T}\tilde{\boldsymbol{H}})^{-1}\tilde{\boldsymbol{H}}^\mathrm{T} \in \mathbb{R}^{N\times N}$, $\boldsymbol{P}_{\tilde{\boldsymbol{J}}} = \tilde{\boldsymbol{J}}(\tilde{\boldsymbol{J}}^\mathrm{T}\tilde{\boldsymbol{J}})^{-1}\tilde{\boldsymbol{J}}^\mathrm{T} \in \mathbb{R}^{N\times N}$ and $\boldsymbol{P}_{\tilde{\boldsymbol{J}}}^\perp = \boldsymbol{I}_N - \boldsymbol{P}_{\tilde{\boldsymbol{J}}}$.

According to the training data, the ML estimate of the persymmetric matrix $\boldsymbol{M}$ can be obtained as [19]

$$\hat{\boldsymbol{M}} = \mathrm{Re}\left(\frac{1}{R}\sum\nolimits_{t=1}^{R}\boldsymbol{y}_t\boldsymbol{y}_t^\mathrm{H}\right) \in \mathbb{R}^{N\times N}, \tag{19}$$

where $\mathrm{Re}\,(\cdot)$ represents the real part of a complex quantity. The constraint $R \geqslant \lceil N/2\rceil$ has to be met to ensure the non-singularity of $\hat{\boldsymbol{M}}$, where $\lceil\cdot\rceil$ represents the smallest integer not smaller than a given parameter. By replacing the unknown matrix $\boldsymbol{M}$ with $\hat{\boldsymbol{M}}$ into (18), we obtain P2S-Rao as

$$\lambda_{\text{P2S-Rao}} = \mathrm{tr}\left(\hat{\boldsymbol{Z}}^\mathrm{H}\boldsymbol{P}_{\hat{\boldsymbol{J}}}^\perp\boldsymbol{P}_{\hat{\boldsymbol{H}}}\boldsymbol{P}_{\hat{\boldsymbol{J}}}^\perp\hat{\boldsymbol{Z}}\right) \underset{\mathrm{H}_0}{\overset{\mathrm{H}_1}{\gtrless}} T_{\text{P2S-Rao}}, \tag{20}$$

where $\lambda_{\text{P2S-Rao}}$ and $T_{\text{P2S-Rao}}$ denote the detection statistic and threshold after replacement, with

$$\begin{cases} \hat{\boldsymbol{Z}} = [\hat{\boldsymbol{z}}_1, \ldots, \hat{\boldsymbol{z}}_K] = \hat{\boldsymbol{M}}^{-1/2}\boldsymbol{Z} \in \mathbb{C}^{N\times K}, \\ \hat{\boldsymbol{H}} = \hat{\boldsymbol{M}}^{-1/2}\boldsymbol{H} \in \mathbb{R}^{N\times p}, \\ \hat{\boldsymbol{J}} = \hat{\boldsymbol{M}}^{-1/2}\boldsymbol{J} \in \mathbb{R}^{N\times q}, \\ \boldsymbol{P}_{\hat{\boldsymbol{H}}} = \hat{\boldsymbol{H}}(\hat{\boldsymbol{H}}^{\mathrm{T}}\hat{\boldsymbol{H}})^{-1}\hat{\boldsymbol{H}}^{\mathrm{T}} \in \mathbb{R}^{N\times N}, \\ \boldsymbol{P}_{\hat{\boldsymbol{J}}}^{\perp} = \boldsymbol{I}_N - \hat{\boldsymbol{J}}(\hat{\boldsymbol{J}}^{\mathrm{T}}\hat{\boldsymbol{J}})^{-1}\hat{\boldsymbol{J}}^{\mathrm{T}} \in \mathbb{R}^{N\times N}. \end{cases} \tag{21}$$

4 CFAR property analyses

In this section, we prove that the proposed P2S-Rao possesses the CFAR property with respect to the clutter covariance matrix and build a process for profiling the proposed detector.

To prove the CFAR property of P2S-Rao, we first rewrite (20) as

$$\lambda_{\text{ P2S-Rao}} = \mathrm{tr}[\boldsymbol{Z}^{\mathrm{H}}\boldsymbol{F}\boldsymbol{H}(\boldsymbol{H}^{\mathrm{T}}\hat{\boldsymbol{M}}^{-1}\boldsymbol{H})^{-1}\boldsymbol{H}^{\mathrm{T}}\boldsymbol{F}\boldsymbol{Z}], \tag{22}$$

where $\boldsymbol{F} = \hat{\boldsymbol{M}}^{-1} - \hat{\boldsymbol{M}}^{-1}\boldsymbol{J}(\boldsymbol{J}^{\mathrm{T}}\hat{\boldsymbol{M}}^{-1}\boldsymbol{J})^{-1}\boldsymbol{J}^{\mathrm{T}}\hat{\boldsymbol{M}}^{-1} \in \mathbb{R}^{N\times N}$. Define $\boldsymbol{J}_{\|} = \boldsymbol{M}^{-1/2}\boldsymbol{J}\left(\boldsymbol{J}^{\mathrm{T}}\boldsymbol{M}^{-1}\boldsymbol{J}\right)^{-1/2} \in \mathbb{R}^{N\times q}$, and then we have $\boldsymbol{J}_{\|}^{\mathrm{T}}\boldsymbol{J}_{\|} = \boldsymbol{I}_q$. There exists an orthogonal matrix $\boldsymbol{U}=\left[\boldsymbol{J}_{\|}, \boldsymbol{J}_{\perp}\right] \in \mathbb{R}^{N\times N}$ with

$$\boldsymbol{J}_{\perp}^{\mathrm{T}}\boldsymbol{J}_{\perp} = \boldsymbol{I}_{N-q} \text{ and } \boldsymbol{J}_{\perp}^{\mathrm{T}}\boldsymbol{J}_{\|} = \boldsymbol{0}_{(N-q)\times q}, \tag{23}$$

where $\boldsymbol{0}_{m\times n}$ denotes an $m\times n$ zero matrix; the $N\times(N-q)$ semi-orthogonal matrix $\boldsymbol{J}_{\perp}$ can be obtained via the singular value decomposition (SVD) of $\widetilde{\boldsymbol{J}}$.

Let

$$\begin{cases} \bar{\boldsymbol{Z}}=\boldsymbol{U}^{\mathrm{T}}\boldsymbol{M}^{-1/2}\boldsymbol{Z} \in \mathbb{C}^{N\times K}, \\ \bar{\boldsymbol{H}}=\boldsymbol{U}^{\mathrm{T}}\boldsymbol{M}^{-1/2}\boldsymbol{H} \in \mathbb{R}^{N\times p}, \\ \bar{\boldsymbol{J}}=\boldsymbol{U}^{\mathrm{T}}\boldsymbol{M}^{-1/2}\boldsymbol{J} \in \mathbb{R}^{N\times q}, \\ \bar{\boldsymbol{F}}=\boldsymbol{U}^{\mathrm{T}}\boldsymbol{M}^{1/2}\boldsymbol{F}\boldsymbol{M}^{1/2}\boldsymbol{U} \in \mathbb{R}^{N\times N}, \\ \bar{\boldsymbol{M}}=\boldsymbol{U}^{\mathrm{T}}\boldsymbol{M}^{-1/2}\hat{\boldsymbol{M}}\boldsymbol{M}^{-1/2}\boldsymbol{U} \in \mathbb{R}^{N\times N}. \end{cases} \tag{24}$$

Then, Eq. (22) can be recast as

$$\lambda_{\text{P2S-Rao}} = \mathrm{tr}\left[\bar{\boldsymbol{Z}}^{\mathrm{H}}\bar{\boldsymbol{F}}\bar{\boldsymbol{H}}\left(\bar{\boldsymbol{H}}^{\mathrm{T}}\bar{\boldsymbol{M}}^{-1}\bar{\boldsymbol{H}}\right)^{-1}\bar{\boldsymbol{H}}^{\mathrm{T}}\bar{\boldsymbol{F}}\bar{\boldsymbol{Z}}\right]. \tag{25}$$

We can verify that under hypothesis H_0, $\bar{\boldsymbol{Z}}$ is distributed as $\bar{\boldsymbol{Z}}\sim\mathcal{CN}\left(\boldsymbol{0}_{N\times K}, \boldsymbol{I}_N\right)$, and it is proven in [19] that $\hat{\boldsymbol{M}}$ is distributed as $\hat{\boldsymbol{M}}\sim\frac{1}{2R}\mathcal{W}\left(2R, \boldsymbol{M}\right)$, where $\mathcal{W}\left(n, \boldsymbol{\Sigma}\right)$ denotes a real Wishart distribution with n degrees of freedom and parameter matrix $\boldsymbol{\Sigma}$. Herein, the matrices are partitioned as $\bar{\boldsymbol{Z}} = \left[\bar{\boldsymbol{Z}}_1^{\mathrm{T}}, \bar{\boldsymbol{Z}}_2^{\mathrm{T}}\right]^{\mathrm{T}}$ with $\bar{\boldsymbol{Z}}_1 \in \mathbb{C}^{q\times K}$ and $\bar{\boldsymbol{Z}}_2 \in \mathbb{C}^{(N-q)\times K}$; $\bar{\boldsymbol{H}} = [\bar{\boldsymbol{H}}_1^{\mathrm{T}}, \bar{\boldsymbol{H}}_2^{\mathrm{T}}]^{\mathrm{T}}$ with $\bar{\boldsymbol{H}}_1 \in \mathbb{R}^{q\times p}$ and $\bar{\boldsymbol{H}}_2 \in \mathbb{R}^{(N-q)\times p}$; $\bar{\boldsymbol{M}} = \left[\begin{smallmatrix}\bar{\boldsymbol{M}}_{11} & \bar{\boldsymbol{M}}_{21}^{\mathrm{T}} \\ \bar{\boldsymbol{M}}_{21} & \bar{\boldsymbol{M}}_{22}\end{smallmatrix}\right]$ with $\bar{\boldsymbol{M}}_{11} \in \mathbb{R}^{q\times q}$, $\bar{\boldsymbol{M}}_{21} \in \mathbb{R}^{(N-q)\times q}$ and $\bar{\boldsymbol{M}}_{22} \in \mathbb{R}^{(N-q)\times(N-q)}$. The inverse of $\bar{\boldsymbol{M}}$ is defined as

$$\bar{\boldsymbol{M}}^{-1} = \begin{bmatrix} \boldsymbol{C}_{11} & \boldsymbol{C}_{12} \\ \boldsymbol{C}_{21} & \boldsymbol{C}_{22} \end{bmatrix}, \tag{26}$$

where $\boldsymbol{C}_{11} \in \mathbb{R}^{q\times q}$, $\boldsymbol{C}_{12} \in \mathbb{R}^{q\times(N-q)}$, $\boldsymbol{C}_{21} \in \mathbb{R}^{(N-q)\times q}$, and $\boldsymbol{C}_{22} \in \mathbb{R}^{(N-q)\times(N-q)}$ are the submatrices of $\bar{\boldsymbol{M}}^{-1}$ defined for convenience. Then, it is straightforward to verify that $\bar{\boldsymbol{F}}$ can be recast as [20]

$$\begin{aligned} \bar{\boldsymbol{F}} &= \boldsymbol{U}^{\mathrm{T}}\boldsymbol{M}^{1/2}[\hat{\boldsymbol{M}}^{-1} - \hat{\boldsymbol{M}}^{-1}\boldsymbol{J}(\boldsymbol{J}^{\mathrm{T}}\hat{\boldsymbol{M}}^{-1}\boldsymbol{J})^{-1}\boldsymbol{J}^{\mathrm{T}}\hat{\boldsymbol{M}}^{-1}]\boldsymbol{M}^{1/2}\boldsymbol{U} \\ &= \bar{\boldsymbol{M}}^{-1} - \bar{\boldsymbol{M}}^{-1}\bar{\boldsymbol{J}}(\bar{\boldsymbol{J}}^{\mathrm{T}}\bar{\boldsymbol{M}}^{-1}\bar{\boldsymbol{J}})^{-1}\bar{\boldsymbol{J}}^{\mathrm{T}}\bar{\boldsymbol{M}}^{-1} \\ &= \bar{\boldsymbol{M}}^{-1} - \bar{\boldsymbol{M}}^{-1}\boldsymbol{E}_0(\boldsymbol{E}_0^{\mathrm{T}}\bar{\boldsymbol{M}}^{-1}\boldsymbol{E}_0)^{-1}\boldsymbol{E}_0^{\mathrm{T}}\bar{\boldsymbol{M}}^{-1} \\ &= \begin{bmatrix} \boldsymbol{0}_{q\times q} & \boldsymbol{0}_{q\times(N-q)} \\ \boldsymbol{0}_{(N-q)\times q} & \bar{\boldsymbol{M}}_{22}^{-1} \end{bmatrix}, \end{aligned} \tag{27}$$

where $\boldsymbol{E}_0 = \left[\boldsymbol{I}_q, \boldsymbol{0}_{q\times(N-q)}\right]^{\mathrm{T}}$, $\bar{\boldsymbol{M}}_{22} = \left(\boldsymbol{C}_{22} - \boldsymbol{C}_{21}\boldsymbol{C}_{11}^{-1}\boldsymbol{C}_{12}\right)^{-1}$, and we have used $\bar{\boldsymbol{J}} = \boldsymbol{E}_0(\boldsymbol{J}^{\mathrm{T}}\boldsymbol{M}^{-1}\boldsymbol{J})^{1/2}$. Substituting (27) into (25), we have

$$\lambda_{\text{P2S-Rao}} = \mathrm{tr}\left[\bar{\boldsymbol{Z}}_2^{\mathrm{H}}\bar{\boldsymbol{M}}_{22}^{-1}\bar{\boldsymbol{H}}_2\left(\bar{\boldsymbol{H}}^{\mathrm{T}}\bar{\boldsymbol{M}}^{-1}\bar{\boldsymbol{H}}\right)^{-1}\bar{\boldsymbol{H}}_2^{\mathrm{T}}\bar{\boldsymbol{M}}_{22}^{-1}\bar{\boldsymbol{Z}}_2\right]. \tag{28}$$

It can be verified that under hypothesis H_0, $\bar{\boldsymbol{Z}}_2$ and $\bar{\boldsymbol{M}}_{22}$ are distributed as $\bar{\boldsymbol{Z}}_2 \sim \mathcal{CN}\left(\boldsymbol{0}_{(N-q)\times K}, \boldsymbol{I}_{N-q}\right)$ and $\bar{\boldsymbol{M}}_{22} \sim \frac{1}{2R}\mathcal{W}\left(2R, \boldsymbol{I}_{N-q}\right)$, respectively. Using the $(N-q)\times p$ matrix $\bar{\boldsymbol{H}}_2$, we can construct a real orthogonal matrix as $\boldsymbol{V} = \left[\bar{\boldsymbol{H}}_{2_\parallel}, \bar{\boldsymbol{H}}_{2_\perp}\right] \in \mathbb{R}^{(N-q)\times(N-q)}$, with $\bar{\boldsymbol{H}}_{2_\parallel} = \bar{\boldsymbol{H}}_2\left(\bar{\boldsymbol{H}}_2^{\mathrm{T}}\bar{\boldsymbol{H}}_2\right)^{-1/2} \in \mathbb{R}^{(N-q)\times p}$ and $\bar{\boldsymbol{H}}_{2_\perp}$ being an $(N-q)\times(N-p-q)$ semi-orthogonal matrix that can be obtained via the SVD of $\bar{\boldsymbol{H}}_2$. Let $\bar{\boldsymbol{Z}}_{2_{\boldsymbol{V}}} = \boldsymbol{V}^{\mathrm{T}}\bar{\boldsymbol{Z}}_2$, $\boldsymbol{E}_1 = [\boldsymbol{I}_p^{\mathrm{T}}, \boldsymbol{0}_{(N-p-q)\times p}^{\mathrm{T}}]^{\mathrm{T}}$, $\bar{\boldsymbol{M}}_{22_{\boldsymbol{V}}} = \boldsymbol{V}^{\mathrm{T}}\bar{\boldsymbol{M}}_{22}\boldsymbol{V}$ [21], and Eq. (28) can be rewritten as

$$\lambda_{\text{P2S-Rao}} = \mathrm{tr}\left[\bar{\boldsymbol{Z}}_{2_{\boldsymbol{V}}}^{\mathrm{H}}\bar{\boldsymbol{M}}_{22_{\boldsymbol{V}}}^{-1}\boldsymbol{E}_1\left(\bar{\boldsymbol{H}}^{\mathrm{T}}\bar{\boldsymbol{M}}^{-1}\bar{\boldsymbol{H}}\right)^{-1}\boldsymbol{E}_1^{\mathrm{T}}\bar{\boldsymbol{M}}_{22_{\boldsymbol{V}}}^{-1}\bar{\boldsymbol{Z}}_{2_{\boldsymbol{V}}}\right], \tag{29}$$

where we have used $\boldsymbol{V}^{\mathrm{T}}\bar{\boldsymbol{H}}_2 = \boldsymbol{E}_1\left(\bar{\boldsymbol{H}}_2^{\mathrm{T}}\bar{\boldsymbol{H}}_2\right)^{1/2}$. Under hypothesis H_0, $\bar{\boldsymbol{Z}}_{2_{\boldsymbol{V}}}$ and $\bar{\boldsymbol{M}}_{22_{\boldsymbol{V}}}$ are distributed as

$$\bar{\boldsymbol{Z}}_{2_{\boldsymbol{V}}} \sim \mathcal{CN}\left(\boldsymbol{0}_{(N-q)\times R}, \boldsymbol{I}_{N-q}\right) \text{ and } \bar{\boldsymbol{M}}_{22_V} \sim \frac{1}{2R}\mathcal{W}\left(2R, \boldsymbol{I}_{N-q}\right), \tag{30}$$

respectively. Using the $N\times p$ matrix $\bar{\boldsymbol{H}}$, we can construct a real orthogonal matrix as $\boldsymbol{W} = \left[\bar{\boldsymbol{H}}_\parallel, \bar{\boldsymbol{H}}_\perp\right] \in \mathbb{R}^{N\times N}$, with $\bar{\boldsymbol{H}}_\parallel = \bar{\boldsymbol{H}}\left(\bar{\boldsymbol{H}}^{\mathrm{T}}\bar{\boldsymbol{H}}\right)^{-1/2} \in \mathbb{R}^{N\times N}$ and $\bar{\boldsymbol{H}}_\perp$ being an $N\times(N-p)$ semi-orthogonal matrix that can be obtained via the SVD of $\bar{\boldsymbol{H}}$. Performing the orthogonal transformation into $\bar{\boldsymbol{H}}$ and $\bar{\boldsymbol{M}}$ in (29) with $\boldsymbol{W}$ yields

$$\lambda_{\text{P2S-Rao}} = \mathrm{tr}\left[\bar{\boldsymbol{Z}}_{2_{\boldsymbol{V}}}^{\mathrm{H}}\bar{\boldsymbol{M}}_{22_{\boldsymbol{V}}}^{-1}\boldsymbol{E}_1\left(\boldsymbol{E}_2^{\mathrm{T}}\bar{\boldsymbol{M}}_{\boldsymbol{W}}^{-1}\boldsymbol{E}_2\right)^{-1}\boldsymbol{E}_1^{\mathrm{T}}\bar{\boldsymbol{M}}_{22_{\boldsymbol{V}}}^{-1}\bar{\boldsymbol{Z}}_{2_{\boldsymbol{V}}}\right], \tag{31}$$

where $\bar{\boldsymbol{M}}_{\boldsymbol{W}} = \boldsymbol{W}^{\mathrm{T}}\bar{\boldsymbol{M}}\boldsymbol{W}$, $\boldsymbol{E}_2 = [\boldsymbol{I}_p^{\mathrm{T}}, \boldsymbol{0}_{(N-p)\times p}^{\mathrm{T}}]^{\mathrm{T}}$, and we have used $\boldsymbol{W}^{\mathrm{T}}\bar{\boldsymbol{H}} = \boldsymbol{E}_2\left(\bar{\boldsymbol{H}}^{\mathrm{T}}\bar{\boldsymbol{H}}\right)^{1/2}$ [21].

It can be verified that under hypothesis H_0, $\bar{\boldsymbol{M}}_{\boldsymbol{W}}$ is distributed as

$$\bar{\boldsymbol{M}}_{\boldsymbol{W}} \sim \frac{1}{2R}\mathcal{W}\left(2R, \boldsymbol{I}_N\right). \tag{32}$$

Remark 1. The results in (30)–(32) show that the P2S-Rao is statistically independent of $\boldsymbol{M}$ under hypothesis H_0; therefore, the proposed P2S-Rao achieves CFAR with respect to $\boldsymbol{M}$.

Next, we build a process for profiling the proposed detector. Eq. (20) can be recast as

$$\lambda_{\text{P2S-Rao}} = \sum_{t=1}^{K}\hat{\boldsymbol{z}}_t^{\mathrm{H}}\boldsymbol{P}_{\hat{\boldsymbol{J}}}^{\perp}\boldsymbol{P}_{\hat{\boldsymbol{H}}}\boldsymbol{P}_{\hat{\boldsymbol{J}}}^{\perp}\hat{\boldsymbol{z}}_t = \sum_{t=1}^{K}\hat{\boldsymbol{z}}_t^{\mathrm{H}}\left(\boldsymbol{P}_{\hat{\boldsymbol{H}}}\boldsymbol{P}_{\hat{\boldsymbol{J}}}^{\perp}\right)^{\mathrm{H}}\boldsymbol{P}_{\hat{\boldsymbol{H}}}\boldsymbol{P}_{\hat{\boldsymbol{J}}}^{\perp}\hat{\boldsymbol{z}}_t = \sum_{t=1}^{K}\left\|\boldsymbol{P}_{\hat{\boldsymbol{H}}}\boldsymbol{P}_{\hat{\boldsymbol{J}}}^{\perp}\hat{\boldsymbol{z}}_t\right\|^2. \tag{33}$$

From (33), it can be observed that there are four procedures in the P2S-Rao (Figure 1). (1) Using the unitary matrix $\boldsymbol{T}$ to transform the test data $\dot{\boldsymbol{z}}_t, t = 1, 2, \ldots, K$ and the training data $\dot{\boldsymbol{y}}_t, t = 1, 2, \ldots, R$, as well as the target signal subspace $\dot{\boldsymbol{H}}$ and the interference subspace $\dot{\boldsymbol{J}}$. (2) Using the ML estimate of $\boldsymbol{M}$ to quasi-whiten the transformed test data $\boldsymbol{z}_t, t = 1, 2, \ldots, K$ and the transformed matrices $\boldsymbol{H}$ and $\boldsymbol{J}$. The aim of this operation is to suppress the colored Gaussian clutter. (3) Projecting the quasi-whitening data onto the complementary space of the quasi-whitened interference subspace using the operator $\boldsymbol{P}_{\hat{\boldsymbol{J}}}^{\perp}$; this operation aims to suppress interference, and then, the operator $\boldsymbol{P}_{\hat{\boldsymbol{H}}}$ is used to integrate the target signal. (4) Finally, the squared Euclidean norm $\|\cdot\|^2$ and the noncoherent integration (i.e., summation) are leveraged to congregate the target energy.

Remark 2. The interference is eliminated in the third procedure, and hence, the proposed P2S-Rao has the capability of interference rejection; that is, the P2S-Rao is insensitive to the interference.

5 Numerical results

In this section, several numerical analyses are conducted to investigate the performance of the proposed P2S-Rao.

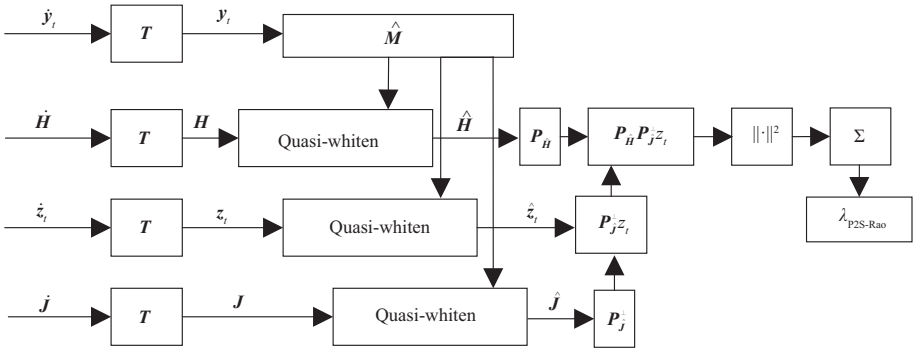

Figure 1 Construction steps of the proposed P2S-Rao.

Table 1 Values of ξ_t for different MDS models

Model number	Range cell number			
	1	2	$\cdots$	$1/h_0$
Model 1	$1/h_0$	$1/h_0$	$1/h_0$	$1/h_0$
Model 2	0.5	$0.5/(h_0-1)$	$0.5/(h_0-1)$	$0.5/(h_0-1)$
Model 3	0.9	$0.1/(h_0-1)$	$0.1/(h_0-1)$	$0.1/(h_0-1)$
Model 4	1	0	0	0

In the Monte Carlo numerical procedure, $100/P_{\text{fa}}$ and 10^4 independent trials are performed to calculate the detection threshold for a preassigned probability of false alarm (P_{fa}) and the probability of detection (P_{d}), respectively. To alleviate computation complexity, we set $P_{\text{fa}} = 10^{-3}$. The subspace matrices $\boldsymbol{H}$ and $\boldsymbol{J}$ can be modeled as those in [14]. $\boldsymbol{P}$ and $\boldsymbol{Q}$ are randomly generated as non-zero matrices. The (i,j)-th element of the clutter covariance matrix is set as $[\boldsymbol{M}]_{i,j} = \sigma_{\text{c}}^2 \rho^{|i-j|}$, where ρ is the clutter one-lag correlation coefficient, and σ_{c}^2 denotes the clutter power level. The signal-to-clutter ratio (SCR) and the interference-to-clutter ratio (ICR) are respectively defined as

$$\text{SCR} = \text{tr}(\boldsymbol{P}^{\text{H}} \dot{\boldsymbol{H}}^{\text{H}} \dot{\boldsymbol{M}}^{-1} \dot{\boldsymbol{H}} \boldsymbol{P})/K, \tag{34}$$

$$\text{ICR} = \text{tr}(\boldsymbol{Q}^{\text{H}} \dot{\boldsymbol{J}}^{\text{H}} \dot{\boldsymbol{M}}^{-1} \dot{\boldsymbol{J}} \boldsymbol{Q})/K. \tag{35}$$

In addition, it is assumed that all K range cells have interference and clutter components, while only the h_0 range cells may have target signal components. Let ξ_t indicate the ratio of target signal energy from the t-th range cell to the total target energy. Herein, four typical models of multiple dominant scatterers (MDSs) are evaluated (Table 1).

5.1 CFAR assessment

To verify the CFAR property of the P2S-Rao, Figure 2 shows the curves of P_{fa} versus detection threshold for different values of σ_{c}^2 and ρ. Four curves with different parameters coincide with each other. This indicates that the proposed detector possesses the CFAR property under the design assumptions, which is consistent with Remark 1.

5.2 Influence of target parameters

Figure 3 shows the curves of P_{d} versus SCR for four typical MDS models from Table 1. When the target signal energy is uniformly distributed in range cells (i.e., Model 1), the P2S-Rao detector performs best, and the detection performance decreases as most of the target energy is nearly concentrated in one range cell. Model 1 is used in the following analyses, except stated otherwise.

Moreover, Figure 4 shows P_{d} versus SCR, with $K = 5, 10, 15, 20$. The performance of the P2S-Rao slightly improves as K increases, but the performance difference is trivial for large K values. In addition, Figure 5 shows the curves of P_{d} versus SCR with $h_0 = 1, 3, 7, 10$. As the value of h_0 increases, the performance of P2S-Rao improves, while the performance gain decreases.

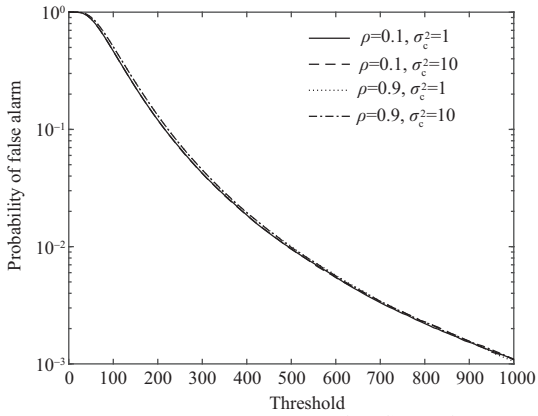

Figure 2 $P_{\rm fa}$ versus the threshold of P2S-Rao for $N = 12$, $K = 15$, $R = 7$, $p = 4$, $q = 4$, ICR = 15 dB.

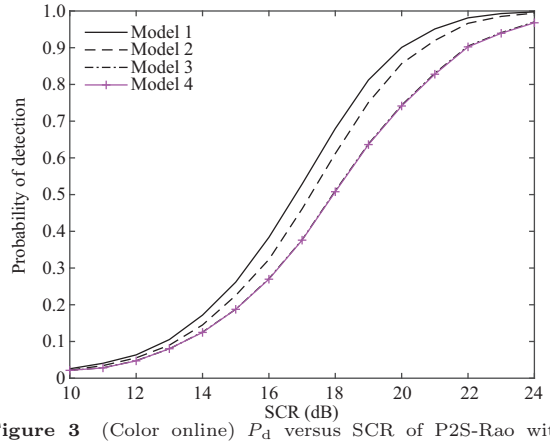

Figure 3 (Color online) $P_{\rm d}$ versus SCR of P2S-Rao with Models 1–4 for $N = 12$, $K = 15$, $R = 7$, $p = 4$, $q = 4$, $P_{\rm fa} = 10^{-3}$, $\rho = 0.9$, $h_0 = 3$, ICR = 15 dB.

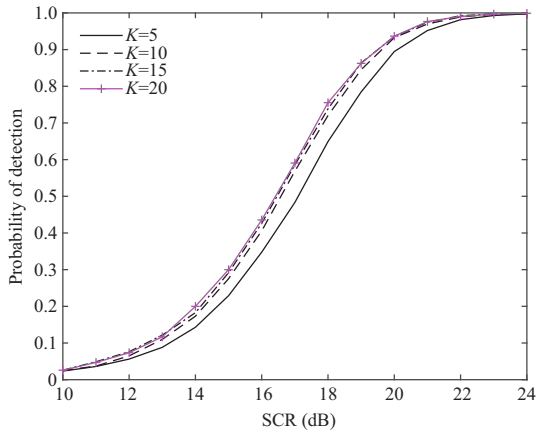

Figure 4 (Color online) $P_{\rm d}$ versus SCR of P2S-Rao with Model 1 for $N = 12$, $K = 5, 10, 15, 20$, $R = 7$, $p = 4$, $q = 4$, $P_{\rm fa} = 10^{-3}$, $\rho = 0.9$, $h_0 = 3$, ICR = 15 dB.

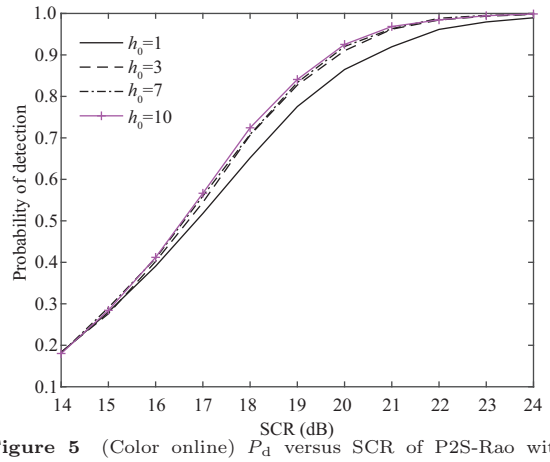

Figure 5 (Color online) $P_{\rm d}$ versus SCR of P2S-Rao with Model 1 for $N = 12$, $K = 15$, $R = 7$, $p = 4$, $q = 4$, $P_{\rm fa} = 10^{-3}$, $\rho = 0.9$, $h_0 = 1, 3, 7, 10$, ICR = 15 dB.

5.3 Influence of interference and clutter parameters

In Figure 6, the $P_{\rm d}$ of P2S-Rao is plotted as a function of SCR, with ICR $= 5, 10, 15, 20$ dB. All curves coincide with each other for different ICRs; that is, the P2S-Rao detector can effectively reject the interference, which is consistent with Remark 2.

Figure 7 refers to the detection performance of P2S-Rao for different numbers of channels ($N = 8, 10, 12, 14$), with R fixed at 7. The performance of P2S-Rao degrades with increasing N, possibly because the dimension of the unknown $\boldsymbol{M}$ depends on the number N, and in the case in which the training data size is fixed, the increase in N will reduce the estimation accuracy of $\boldsymbol{M}$, thereby deteriorating the detection performance. Figure 8 shows the curves of $P_{\rm d}$ versus SCR, with $N = 8, 12, 16, 20$; R is always equal to N. The P2S-Rao performance is enhanced as N increases, with the constraint of $N = R$.

In addition, Figure 9 shows $P_{\rm d}$ of P2S-Rao versus SCR with $R = 8, 16, 24, 32$. As R increases, the detection performance improves because a larger R leads to a more accurate estimate of $\boldsymbol{M}$. In Figure 10, the detection performance of P2S-Rao is demonstrated for different clutter one-lag correlation coefficients. The nearly superposed curves show that the P2S-Rao performs robustly for different clutter correlations.

5.4 Performance comparison

We compare the proposed P2S-Rao with the existing unstructured subspace detectors, including 1S-GLRT [11], 2S-GLRT [11], 1S-Rao [12], 2S-Rao [12], and MRao [13], and the existing structured P1S-GLRT [14]. In [14], the P1S-GLRT generally outperformed the two-step one; herein we only consider the P1S-GLRT owing to space limitations.

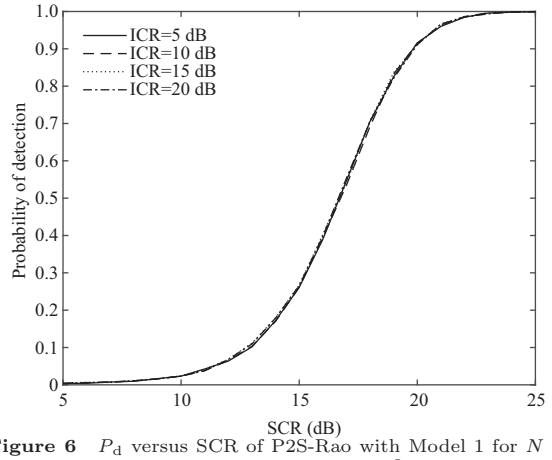

Figure 6 $P_{\rm d}$ versus SCR of P2S-Rao with Model 1 for $N = 12$, $K = 15$, $R = 7$, $p = 4$, $q = 4$, $P_{\rm fa} = 10^{-3}$, $\rho = 0.9$, $h_0 = 3$, ICR $= 5, 10, 15, 20$ dB.

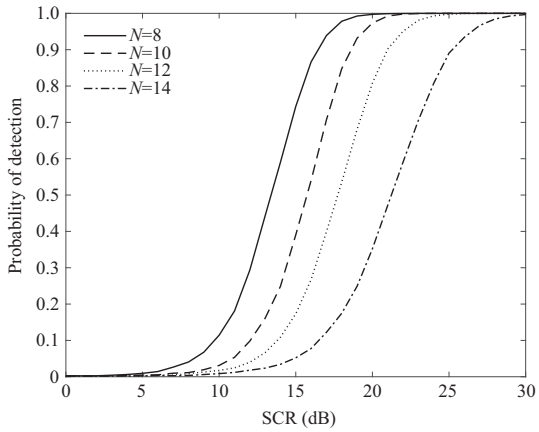

Figure 7 $P_{\rm d}$ versus SCR of P2S-Rao with Model 1 for $N = 8, 10, 12, 14$, $K = 15$, $R = 7$, $p = 4$, $q = 4$, $P_{\rm fa} = 10^{-3}$, $\rho = 0.9$, $h_0 = 3$, ICR $= 15$ dB.

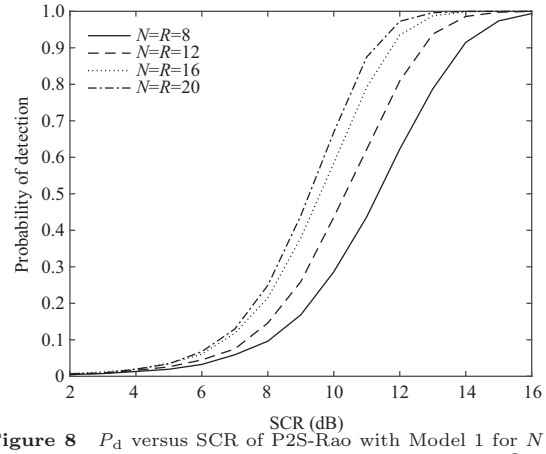

Figure 8 $P_{\rm d}$ versus SCR of P2S-Rao with Model 1 for $N = R = 8, 12, 16, 20$, $K = 15$, $R = 7$, $p = 4$, $q = 4$, $P_{\rm fa} = 10^{-3}$, $\rho = 0.9$, $h_0 = 3$, ICR $= 15$ dB.

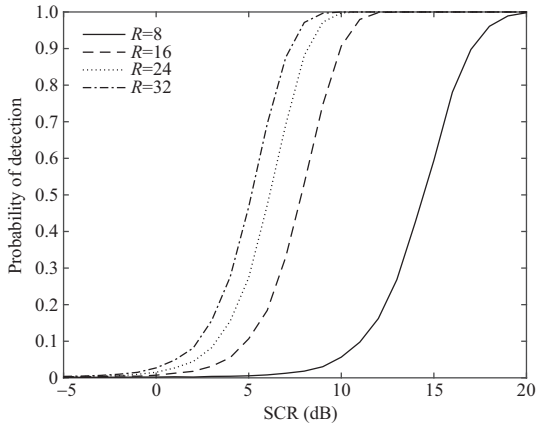

Figure 9 $P_{\rm d}$ versus SCR of P2S-Rao with Model 1 for $N = 12$, $K = 15$, $R = 8, 16, 24, 32$, $p = 4$, $q = 4$, $P_{\rm fa} = 10^{-3}$, $\rho = 0.9$, $h_0 = 3$, ICR $= 15$ dB.

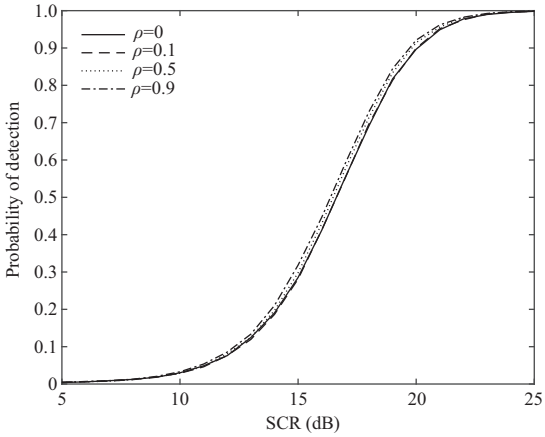

Figure 10 $P_{\rm d}$ versus SCR of P2S-Rao with Model 1 for $N = 12$, $K = 15$, $R = 7$, $p = 4$, $q = 4$, $P_{\rm fa} = 10^{-3}$, $\rho = 0, 0.1, 0.5, 0.9$, $h_0 = 3$, ICR $= 15$ dB.

First, we consider the computational complexity of different detectors. The observed data from range cells are complex-valued, but the matrices $\boldsymbol{H}$, $\boldsymbol{J}$ and $\boldsymbol{M}$ are real-valued after the unitary transformation $\boldsymbol{T}$. In the case in which the persymmetry is not considered or the transforming procedure in [14] is used, all data and variables are still complex-valued. For the computational complexity discussed herein, the impact of the addition operation is ignored in each decision-making process, and only the actual

Table 2 Computational complexity of different detectors

Detector	Detection statistics	Computational complexity
P2S-Rao	$\mathrm{tr}(\boldsymbol{W}_1)$	$N^3+N^2(4K+8R+6p+6q)+N(2K^2+p^2+2q^2+3Kp)+Kp^2+p^3+q^3$
P1S-GLRT	$\boldsymbol{W}_6$	$12N^3+4N^2(5K+R+2p+4q)+4N[8K^2+2(p+q)^2+2q^2]+4(p+q)^3+4q^3+4(2K)!+64K^3$
1S-Rao	$\mathrm{tr}[\boldsymbol{W}_2^{-1}\boldsymbol{W}_3(\boldsymbol{W}_2-\boldsymbol{W}_3)^{-1}]$	$8N^3+4N^2(K+2R+2p+4q)+4N(2K^2+p^2+4q^2+2Kp)+16K^3+4p^3+8q^3+4Kp^2$
2S-Rao	$\mathrm{tr}(\boldsymbol{W}_3)$	$4N^3+4N^2(R+2p+2q)+4N(K^2+p^2+2q^2+2Kp)+4p^3+4q^3+4Kp^2$
MRao	$\mathrm{tr}[\boldsymbol{W}_2^{-1}\boldsymbol{W}_5(\boldsymbol{W}_2-\boldsymbol{W}_5)^{-1}]$	$12N^3+4N^2(3K+3R+2p+6q)+4N[3K^2+2(p+q)2+4q^2]+16K^3+4(p+q)^3+8q^3$
1S-GLRT	$\mathrm{tr}(\boldsymbol{W}_2\boldsymbol{W}_4^{-1})$	$8N^3+4N^2(2K+2R+2p+4q)+4N[2K^2+2(p+q)^2+2q^2]+4(p+q)^3+4q^3+4K!+8K^3$
2S-GLRT	$\mathrm{tr}(\boldsymbol{W}_2-\boldsymbol{W}_4)$	$8N^3+4N^2(2K+2R+2p+4q)+4N[2K^2+2(p+q)^2+2q^2]+4(p+q)^3+4q^3$

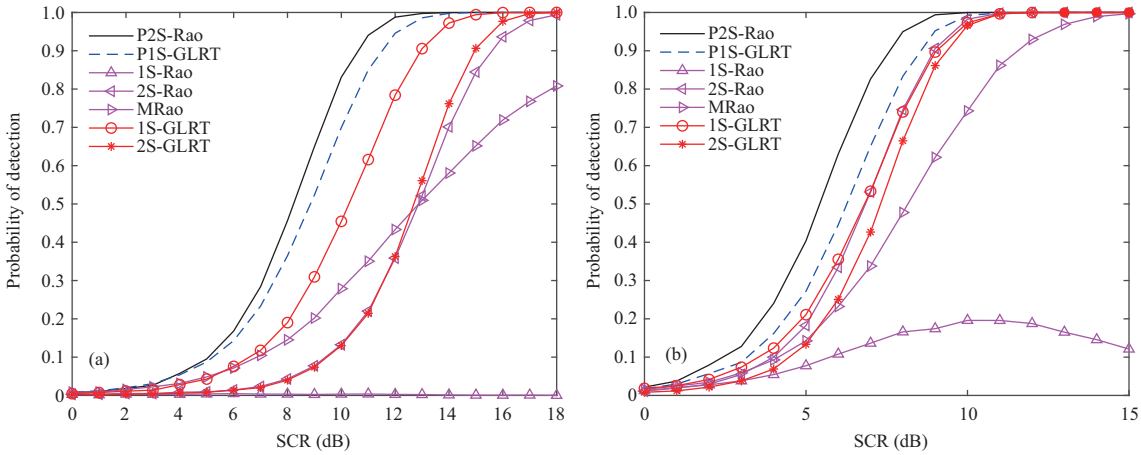

Figure 11 (Color online) P_{d} versus SCR of different detectors with Model 1 for $N=12$, $K=15$, $R=13,24$, $p=4$, $q=4$, $P_{\mathrm{fa}}=10^{-3}$, $\rho=0.9$, $h_0=3$, ICR = 15 dB. (a) $R=13$; (b) $R=24$.

real-valued multiplication is considered.

For easy expression of detection statistics, let

$$\begin{cases} \boldsymbol{W}_1=\hat{\boldsymbol{Z}}^{\mathrm{H}}\boldsymbol{P}_{\hat{\boldsymbol{J}}}^{\perp}\boldsymbol{P}_{\hat{\boldsymbol{H}}}\boldsymbol{P}_{\hat{\boldsymbol{J}}}^{\perp}\hat{\boldsymbol{Z}}\in\mathbb{C}^{K\times K}, \\ \boldsymbol{W}_2=\boldsymbol{I}_K+\tilde{\boldsymbol{Z}}^{\mathrm{H}}\boldsymbol{P}_{\tilde{\boldsymbol{J}}}^{\perp}\tilde{\boldsymbol{Z}}\in\mathbb{C}^{K\times K}, \\ \boldsymbol{W}_3=\tilde{\boldsymbol{Z}}^{\mathrm{H}}\boldsymbol{P}_{\tilde{\boldsymbol{J}}}^{\perp}\boldsymbol{P}_{\tilde{\boldsymbol{H}}}\boldsymbol{P}_{\tilde{\boldsymbol{J}}}^{\perp}\tilde{\boldsymbol{Z}}\in\mathbb{C}^{K\times K}, \\ \boldsymbol{W}_4=\boldsymbol{I}_K+\tilde{\boldsymbol{Z}}^{\mathrm{H}}\boldsymbol{P}_{\tilde{\boldsymbol{B}}}^{\perp}\tilde{\boldsymbol{Z}}\in\mathbb{C}^{K\times K}, \\ \boldsymbol{W}_5=\tilde{\boldsymbol{Z}}^{\mathrm{H}}(\boldsymbol{P}_{\tilde{\boldsymbol{B}}}-\boldsymbol{P}_{\tilde{\boldsymbol{J}}})\tilde{\boldsymbol{Z}}\in\mathbb{C}^{K\times K}, \\ \boldsymbol{W}_6=\det(\boldsymbol{I}_{2K}+\vec{\boldsymbol{Z}}^{\mathrm{H}}\vec{\boldsymbol{P}}_1\vec{\boldsymbol{Z}})/\det(\boldsymbol{I}_{2K}+\vec{\boldsymbol{Z}}^{\mathrm{H}}\vec{\boldsymbol{P}}_2\vec{\boldsymbol{Z}})\in\mathbb{C}^{1\times 1}, \end{cases} \tag{36}$$

where $\vec{\boldsymbol{P}}_1=\vec{\boldsymbol{M}}^{-1}-\vec{\boldsymbol{M}}^{-1}\dot{\boldsymbol{J}}(\dot{\boldsymbol{J}}^{\mathrm{H}}\vec{\boldsymbol{M}}^{-1}\dot{\boldsymbol{J}})^{-1}\dot{\boldsymbol{J}}^{\mathrm{H}}\vec{\boldsymbol{M}}^{-1}\in\mathbb{C}^{N\times N}$ with $\vec{\boldsymbol{M}}=[\dot{\boldsymbol{Y}}\dot{\boldsymbol{Y}}^{\mathrm{H}}+\boldsymbol{D}_N(\dot{\boldsymbol{Y}}\dot{\boldsymbol{Y}}^{\mathrm{H}})^{*}\boldsymbol{D}_N]/2\in\mathbb{C}^{N\times N}$, $\vec{\boldsymbol{P}}_2=\vec{\boldsymbol{M}}^{-1}-\vec{\boldsymbol{M}}^{-1}\dot{\boldsymbol{B}}(\dot{\boldsymbol{B}}^{\mathrm{H}}\vec{\boldsymbol{M}}^{-1}\dot{\boldsymbol{B}})^{-1}\dot{\boldsymbol{B}}^{\mathrm{H}}\vec{\boldsymbol{M}}^{-1}\in\mathbb{C}^{N\times N}$, $\vec{\boldsymbol{Z}}=[\vec{\boldsymbol{Z}}_{\mathrm{e}},\vec{\boldsymbol{Z}}_{\mathrm{o}}]\in\mathbb{C}^{N\times 2K}$ with $\vec{\boldsymbol{Z}}_{\mathrm{e}}=(\dot{\boldsymbol{Z}}+\boldsymbol{D}_N\dot{\boldsymbol{Z}}^{*})/2\in\mathbb{C}^{N\times K}$ and $\vec{\boldsymbol{Z}}_{\mathrm{o}}=(\dot{\boldsymbol{Z}}-\boldsymbol{D}_N\dot{\boldsymbol{Z}}^{*})/2\in\mathbb{C}^{N\times K}$, $\boldsymbol{P}_{\tilde{\boldsymbol{B}}}=\tilde{\boldsymbol{B}}(\tilde{\boldsymbol{B}}^{\mathrm{H}}\tilde{\boldsymbol{B}})^{-1}\tilde{\boldsymbol{B}}^{\mathrm{H}}$ and $\boldsymbol{P}_{\tilde{\boldsymbol{B}}}^{\perp}=\boldsymbol{I}_N-\boldsymbol{P}_{\tilde{\boldsymbol{B}}}$.

Table 2 lists the computational complexities for different detectors. Considering the constraint relationships of $p+q<N$ and $R\geqslant N$, the P2S-Rao exhibits a smaller computational complexity than most of the unstructured detectors (except 2S-Rao) and the structured P1S-GLRT.

Figure 11 compares the P2S-Rao with the unstructured subspace detectors and the P1S-GLRT for different R values. The P2S-Rao outperforms the unstructured subspace detectors for different numbers of training data, which indicates that leveraging the persymmetric structure of the clutter covariance matrix can result in a distinct gain in the detection performance of P2S-Rao. Moreover, the proposed P2S-Rao offers a higher probability of detection than the structured P1S-GLRT under the assumptions of this paper.

In Figure 12, the P_{d}s of P2S-Rao and the other above-mentioned detectors are plotted as a function of P_{fa} in the small sample case. The P2S-Rao can effectively control the probability of false alarms. The P2S-Rao can achieve the same probability of detection with a lower probability of false alarm than the other detectors. For example, to achieve a probability of detection not smaller than 0.8, the probability of a false alarm is approximately 10^{-3} for P2S-Rao; this value is significantly higher for other detectors.

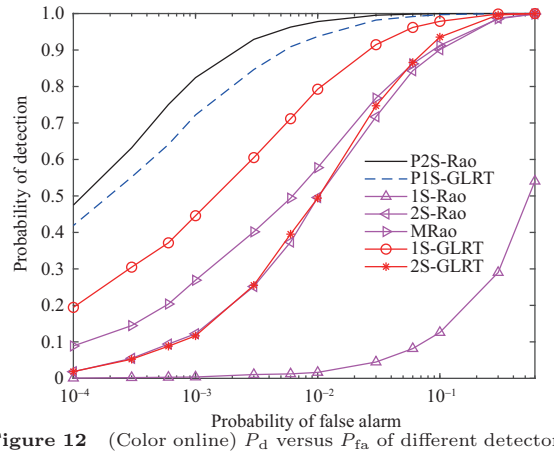

Figure 12 (Color online) P_{d} versus P_{fa} of different detectors with Model 1 for $N = 12$, $K = 15$, $R = 13$, $p = 4$, $q = 4$, $P_{\mathrm{fa}} = 10^{-3}$, $\rho = 0.9$, $h_0 = 3$, ICR = 15 dB, SCR = 10 dB.

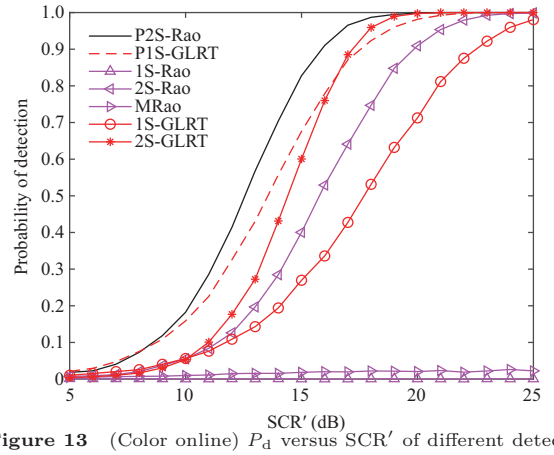

Figure 13 (Color online) P_{d} versus SCR′ of different detectors with Model 1 for $N = 12$, $K = 15$, $R = 13$, $p = 4$, $q = 4$, $P_{\mathrm{fa}} = 10^{-3}$, $\rho = 0.9$, $h_0 = 3$, ICR = 15 dB, $\cos^2\phi = 0.5$.

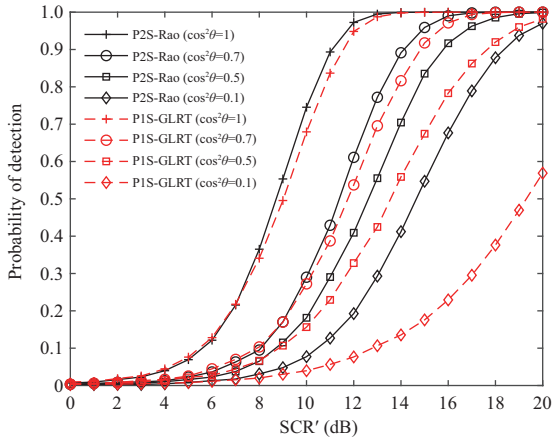

Figure 14 (Color online) P_{d} versus SCR′ of P2S-Rao and P1S-GLRT with Model 1 for $N = 12$, $K = 15$, $R = 13$, $p = 4$, $q = 4$, $P_{\mathrm{fa}} = 10^{-3}$, $\rho = 0.9$, $h_0 = 3$, ICR = 15 dB, $\cos^2\phi = 1, 0.7, 0.5, 0.1$.

In practical applications, owing to several factors such as wavefront distortions and array calibration errors, the nominal signal subspace matrix $\dot{\boldsymbol{H}}$ may deviate from the actual signal subspace matrix $\ddot{\boldsymbol{H}}$. The mismatch case is discussed herein. The mismatch angle ϕ can be defined as [22]

$$\cos^2\phi = \frac{\left|\mathrm{tr}(\ddot{\boldsymbol{H}}^{\mathrm{H}}\dot{\boldsymbol{M}}^{-1}\dot{\boldsymbol{H}})\right|^2}{\mathrm{tr}(\ddot{\boldsymbol{H}}^{\mathrm{H}}\dot{\boldsymbol{M}}^{-1}\ddot{\boldsymbol{H}})\mathrm{tr}(\dot{\boldsymbol{H}}^{\mathrm{H}}\dot{\boldsymbol{M}}^{-1}\dot{\boldsymbol{H}})} \tag{37}$$

which is the squared cosine of the angle between the actual signal subspace $\ddot{\boldsymbol{H}}$ and the nominal value $\dot{\boldsymbol{H}}$ in the whitening space.

The signal-to-clutter ratio in the mismatched case can be expressed as

$$\mathrm{SCR}' = \mathrm{tr}(\boldsymbol{P}^{\mathrm{H}}\ddot{\boldsymbol{H}}^{\mathrm{H}}\dot{\boldsymbol{M}}^{-1}\ddot{\boldsymbol{H}}\boldsymbol{P})/K. \tag{38}$$

Figure 13 shows the P_{d}s of different detectors versus SCR′ for the typical value $\cos^2\phi = 0.5$. All of the detectors suffer performance penalties in the presence of a mismatch, but the P2S-Rao still outperforms the other detectors. Furthermore, different detectors are compared for different mismatch cases in Figure 14. To avoid jampacking too many curves in the graph, we only select P1S-GLRT for comparison because both P2S-Rao and P1S-GLRT almost outperform the other detectors (Figure 13). Particularly, $\cos^2\phi = 1$ indicates the matched case. The two detectors both suffer performance degradation with increasing mismatch; nevertheless, the proposed P2S-Rao outperforms the P1S-GLRT in all cases.

6 Conclusion

By leveraging the persymmetric structure of the clutter covariance matrix, this paper designs the P2S-Rao for the adaptive detection of range-spread targets embedded in subspace interference plus unknown Gaussian clutter. Theoretical analyses show that the proposed P2S-Rao possesses the CFAR property with respect to the clutter covariance matrix and features less computational complexity than the considered competitors. The numerical results show that the P2S-Rao can effectively reject the interference and outperform the unstructured subspace competitors in both matched and mismatched cases. Moreover, the P2S-Rao outperforms the existing persymmetric P1S-GLRT.

Acknowledgements This work was supported by National Natural Science Foundation of China (Grant Nos. 61971432, 61790551), Taishan Scholar Project of Shandong Province (Grant No. tsqn201909156), Outstanding Youth Innovation Team Program of University in Shandong Province (Grant No. 2019KJN031), and Technical Areas Foundation for Fundamental Strengthening Program (Grant No. 2019-JCJQ-JJ-060). The authors would like to thank the anonymous reviewers for their valuable comments and suggestions that helped to greatly improve the quality of the paper.

References

1 Hao C P, Orlando D, Foglia G, et al. Persymmetric adaptive detection of distributed targets in partially-homogeneous environment. Digit Signal Process, 2014, 24: 42–51
2 Shuai X F, Kong L J, Yang J Y. Adaptive detection for distributed targets in Gaussian noise with Rao and Wald tests. Sci China Inf Sci, 2012, 55: 1290–1300
3 Xu S W, Shui P L, Cao Y H. Adaptive range-spread maneuvering target detection in compound-Gaussian clutter. Digit Signal Process, 2015, 36: 46–56
4 Cui G L, Kong L J, Yang X B, et al. Distributed target detection with polarimetric MIMO radar in compound-Gaussian clutter. Digit Signal Process, 2012, 22: 430–438
5 Wang Z, Zhao Z, Ren C, et al. Adaptive detection of distributed targets in noise and interference which is partially related with targets. Digit Signal Process, 2020, 103: 102757
6 Liu W J, Liu J, Hao C P, et al. Multichannel adaptive signal detection: basic theory and literature review. Sci China Inf Sci, 2022, 65: 121301
7 Gao Y C, Ji H B, Liu W J. Persymmetric adaptive subspace detectors for range-spread targets. Digit Signal Process, 2019, 89: 116–123
8 Xiao L, Liu Y M, Huang T Y, et al. Distributed target detection with partial observation. IEEE Trans Signal Process, 2018, 66: 1551–1565
9 Li W J, Tong H B, Li K, et al. Wald tests for direction detection in noise and interference. Multidim Syst Sign Process, 2017, 29: 1563–1577
10 Gao Y C, Liao G S, Liu W J, et al. Bayesian generalised likelihood ratio tests for distributed target detection in interference and noise. IET Radar Sonar & Navigation, 2017, 11: 752–758
11 Bandiera F, de Maio A, Greco A S, et al. Adaptive radar detection of distributed targets in homogeneous and partially homogeneous noise plus subspace interference. IEEE Trans Signal Process, 2007, 55: 1223–1237
12 Liu W J, Liu J, Huang L, et al. Rao tests for distributed target detection in interference and noise. Signal Process, 2015, 117: 333–342
13 Wang Z Z. Modified Rao test for distributed target detection in interference and noise. Signal Process, 2020, 172: 107578
14 Liu J, Jian T, Liu W. Persymmetric detection of subspace signals based on multiple observations in the presence of subspace interference. Signal Process, 2021, 183: 107964
15 Liu J, Liu W J, Tang B, et al. Persymmetric adaptive detection in subspace interference plus Gaussian noise. Signal Process, 2020, 167: 107316
16 Liu J, Sun S Y, Liu W J. One-step persymmetric GLRT for subspace signals. IEEE Trans Signal Process, 2019, 67: 3639–3648
17 Liu W J, Wang Y L, Xie W C. Fisher information matrix, Rao test, and Wald test for complex-valued signals and their applications. Signal Process, 2014, 94: 1–5
18 Liu J, Zhang Z J, Yang Y, et al. A CFAR adaptive subspace detector for first-order or second-order Gaussian signals based on a single observation. IEEE Trans Signal Process, 2011, 59: 5126–5140
19 Pailloux G, Forster P, Ovarlez J P, et al. Persymmetric adaptive radar detectors. IEEE Trans Aerosp Electron Syst, 2011, 47: 2376–2390
20 Liu W J, Wang Y L, Liu J, et al. Performance analysis of adaptive detectors for point targets in subspace interference and Gaussian noise. IEEE Trans Aerosp Electron Syst, 2018, 54: 429–441
21 Liu W J, Liu J, Li H, et al. Multichannel signal detection based on wald test in subspace interference and Gaussian noise. IEEE Trans Aerosp Electron Syst, 2019, 55: 1370–1381
22 Wang Z Z, Zhao Z Q, Ren C H, et al. Adaptive GLR-, Rao- and Wald-based CFAR detectors for a subspace signal embedded in structured Gaussian interference. Digit Signal Process, 2019, 92: 139–150